

# QFold: Quantum Walks and Deep Learning to Solve Protein Folding

P. A. M. Casares,<sup>1,\*</sup> Roberto Campos,<sup>1,2,†</sup> and M. A. Martín-Delgado<sup>1,3,‡</sup>

<sup>1</sup>*Departamento de Física Teórica, Universidad Complutense de Madrid.*

<sup>2</sup>*Quasar Science Resources, SL.*

<sup>3</sup>*CCS-Center for Computational Simulation, Universidad Politécnica de Madrid.*

(Dated: April 23, 2022)

We develop quantum computational tools to predict how proteins fold in 3D, one of the most important problems in current biochemical research. We explain how to combine recent deep learning advances with the well known technique of quantum walks applied to a Metropolis algorithm. The result, QFold, is a fully scalable hybrid quantum algorithm that in contrast to previous quantum approaches does not require a lattice model simplification and instead relies on the much more realistic assumption of parameterization in terms of torsion angles of the amino acids. We compare it with its classical analog for different annealing schedules and find a polynomial quantum advantage, and validate a proof-of-concept realization of the quantum Metropolis in IBMQ Casablanca quantum processor.

## I. INTRODUCTION

Proteins are complex biomolecules, made up of one or several chains of amino acids, and with a large variety of functions in organisms. Amino acids are 20 compounds made of amine ( $-NH_2$ ) and carboxyl ( $-COOH$ ) groups, with a side chain that differentiates them. However, the function of the protein is not only determined by the amino acid chain, which is relatively simple to figure out experimentally, but from its spatial folding, which is much more challenging and expensive to obtain in a laboratory. In fact it is so complicated that the gap between proteins whose sequence is known and those for which the folding structure has been additionally analyzed is three orders of magnitude: there are over 200 million sequences available at the UniProt database [1], but just over 172 thousand whose structure is known, as given in the Protein Data Bank [2]. Furthermore, experimental techniques cannot always analyse the tridimensional configuration of the proteins, giving rise to what is called the dark proteome [3] that represents a significant fraction of the organisms including humans [4, 5]. There are even proteins with several stable foldings [6], and others that have no stable folding called Intrinsically Disordered [7].

Since proteins are such cornerstone biomolecules, and retrieving their folding so complicated, the problem of protein folding is widely regarded as one of the most important and hard problems in computational biochemistry, and has motivated research for decades. Having an efficient and reliable computational procedure to guess their structure would

therefore represent a large boost for biochemical research.

Until recently, one of the most popular approaches to fold proteins was to apply a Metropolis algorithm parameterised in terms of the torsion angles, as is done for example in the popular library package Rosetta [8] and the distributed computing project Rosetta@Home [9, 10]. The main problem with this approach, though, is that the problem is combinatorial in nature, and NP complete even for simple models [11, 12]. For this reason, other approaches are also worth exploring. In the 2018 edition of the Critical Assessment of Techniques for Protein Structure Prediction (CASP) competition [13], for example, the winner was DeepMind’s AlphaFold model [14], that was able to show that Deep Learning techniques allow to obtain much better results. DeepMind approach consisted on training a neural network to produce a mean field potential, dependent on the distance between amino acids and the torsion angles, that can be later minimized by gradient descent.

In this article we study how Quantum Computing could help improve the state of the art in this problem when large error-corrected quantum computers become available. We propose using the prediction of AlphaFold as a starting point for a quantum Metropolis-Hastings algorithm. The Metropolis algorithm is a Markov-chain Monte Carlo algorithm, that is, an algorithm that performs a random walk  $\mathcal{W}$  over a given graph. The Metropolis algorithm is specially designed to quickly reach the equilibrium state, the state  $\pi^\beta$  such that  $\mathcal{W}\pi^\beta = \pi^\beta$ . Slowly modifying the inverse temperature parameter  $\beta$  such that the states with smaller energy become increasingly favoured by the random walk, we should end in the ground state of the system with high probability.

Several modifications of the Metropolis-Hastings algorithm to adapt it to a quantum algorithm have

\* [pabloamo@ucm.es](mailto:pabloamo@ucm.es)

† [robecamp@ucm.es](mailto:robecamp@ucm.es)

‡ [mardel@ucm.es](mailto:mardel@ucm.es)

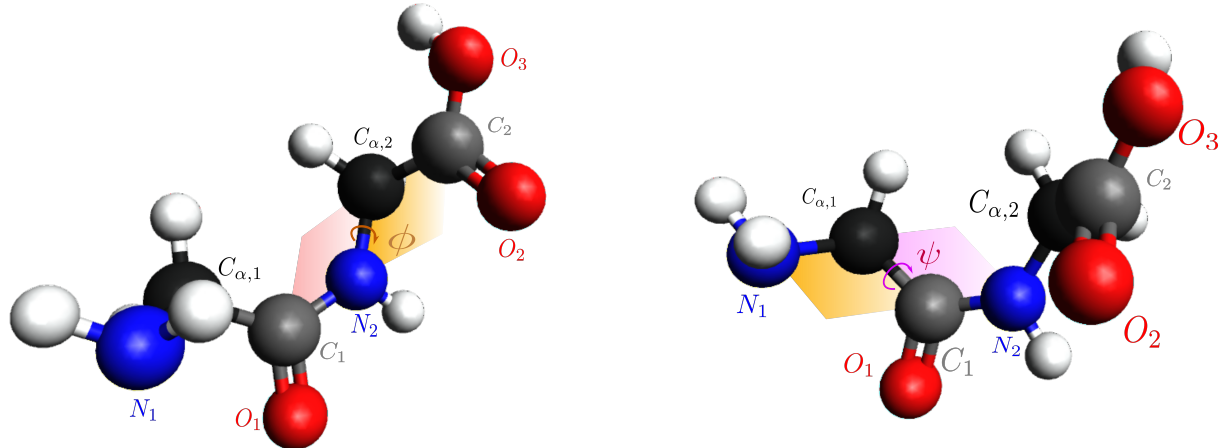


FIG. 1. Example of the smallest dipeptide: the glycylglycine. We can see that each amino acid has the chain (Nitrogen- $C_\alpha$ -Carboxy). Different amino acids would have a different side chain attached to the  $C_\alpha$  instead of Hydrogen as it is the case for the Glycine. In each figure we depict either angle  $\phi$  or  $\psi$ . Angle  $\psi$  is defined as the torsion angle between two planes: the first one defined by the three atoms in the backbone of the amino acid ( $N_1$ ,  $C_{\alpha,1}$ ,  $C_1$ ), and the second by the same atoms except substituting the Nitrogen in that amino acid by the Nitrogen of the subsequent one: ( $C_{\alpha,1}$ ,  $C_1$ ,  $N_2$ ). For the  $\phi$  angle the first plane is made out of the three atoms in the amino acid ( $N_2$ ,  $C_{\alpha,2}$ ,  $C_2$ ) whereas the second plane is defined substituting the Carboxy atom in the amino acid by the Carboxy from the preceding amino acid: ( $C_1$ ,  $N_2$ ,  $C_{\alpha,2}$ ). These graphics were generated using [15] and Inkscape.

been proposed [16–21], mostly based on substituting the classical random walk by a Szegedy quantum walk [22]. On the contrary, our work takes advantage of the application of a quantum Metropolis algorithm under out-of-equilibrium conditions similar to what is usually done classically, and has been done on Ising models[21]. Specifically, we aim to simulate this procedure for several small peptides, the smallest proteins with only a few amino acids; and compare the expected running time with the classical simulated annealing, and also check whether starting from the initial state proposed by an algorithm similar to AlphaFold may speed up the simulated annealing process.

Our work benefits from two different lines of research. The first one makes use of quantum walks to obtain polynomial quantum advantages, inspired mainly by Szegedy work [22], and by theoretical quantum Metropolis algorithms indicated in the above. In contrast with [21], our work focuses only on the unitary heuristic implementation of the Metropolis algorithm, but studies what happens with a different system (peptides) and with different annealing schedules instead of only testing a single linear schedule for the inverse temperature  $\beta$ . Lastly, we also validate a proof of concept using IBM Casablanca processor, experimentally realizing the quantum Metropolis algorithm in actual quantum hardware.

The second line of research related to our work is

the use of quantum techniques to speedup or improve the process of protein folding. The reason for this is because even simplified models of protein folding are NP hard combinatorial optimization problems, so polynomial speedups could in principle be expected from the use of quantum computing instead of their classical counterparts. The literature on this problem [23–29] and related ones [30, 31] focuses on such simplified lattice models that are still very hard, and mostly on adiabatic computation. In contrast, our work presents much more realistic fully scalable model, parametrized in terms of the torsion angles. The torsion angles, also called dihedral, are angles between the atoms in the backbone structure of the protein, that determine its folding. An example with the smallest of the dipeptides, the glycylglycine, can be found in figure 1. These angles are usually three per amino acid,  $\phi$ ,  $\psi$  and  $\omega$ , but the latter is almost always fixed at value  $\pi$  and for that reason, not commonly taken into account in the models [14].

These considerations, and the fact that we use a distilled version of AlphaFold [14] as initialization, makes our work different from the usual approach in quantum protein folding: commonly adiabatic approaches have been used so far, whereas our algorithm is digital. The downside of this more precise approach is that the number of amino acids that we are able to simulate is more restricted, but we are nevertheless able to perform experiments in actual

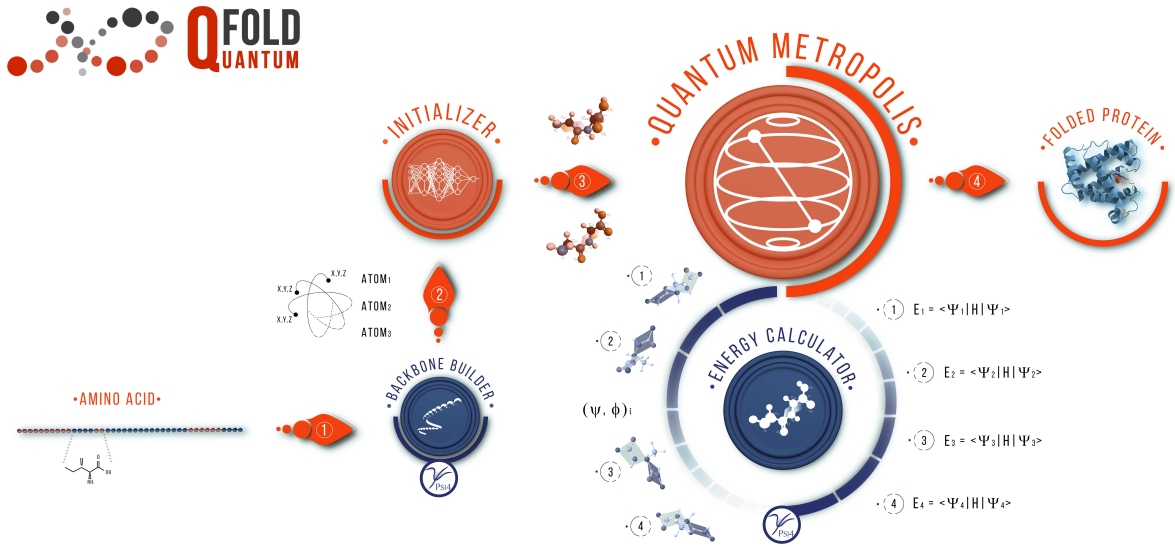


FIG. 2. Scheme of the QFold algorithm. Starting from the amino acid sequence, we use *Psi4* to extract the atoms conforming the protein, and a *Minifold* module, in substitution of AlphaFold, as initializer. The algorithm then uses the guessed angles by *Minifold* as a starting point (or rather, as the means of the starting von Mises distributions with  $\kappa = 1$ ), and the energy of all possible positions calculated by *Psi4*, to perform a quantum Metropolis algorithm that finally outputs the torsion angles. In the scheme of the algorithm, the backbone builder represents a subroutine that recovers the links between atoms of the protein, and in particular the backbone chain, using the atom positions obtained from *PubChem* using *Psi4*. The initializer, instantiated in our case by *Minifold*, is a second subroutine that gives a first estimate of the torsion angles, before passing it to the quantum Metropolis. The energy calculator uses *Psi4* to calculate the energy of all possible rotation angles that we want to explore, and these energies are used in the quantum Metropolis algorithm, which outputs the expected folding. For a more detailed flowchart, we refer to the figure 3.

hardware. Finally, it is worth mentioning that in the 2020 CASP competition, DeepMind’s team tested their AlphaFold v2 algorithm which significantly improves the results from their previous version.

In summary, the main contributions of our work are threefold: firstly, we design a quantum algorithm that is scalable and realistic, and provided with a fault-tolerant quantum computer could become competitive with current state of the art techniques. Secondly, we analyse the use of different cooling schedules in out-of-equilibrium quantum walks, and perform ideal quantum simulations of QFold and compare its performance with the equivalent classical Metropolis algorithm, pointing towards a quantum speedup. This quantum advantage is enough to make the quantum Metropolis more convenient than its classical counterpart in average-length proteins even after taking into account slowdowns due to error correction protocols. Thirdly, we implement a proof-of-concept of the quantum Metropolis algorithm in actual quantum hardware, validating our work.

## II. QFOLD ALGORITHM

The algorithm we introduce is called QFold and has three main components that we will introduce in this section (see figure 2 for a scheme of QFold): an initialization routine to find a good initial guess of the dihedral angles that characterise the protein folding, a quantum Metropolis to find an even lower energy state from the initial guess, and a classical metropolis to compare against the quantum Metropolis to assess possible speedups. The aim of this section is to introduce the theoretical background we have used for our results.

### A. Initializer

QFold makes use of quantum walks as a resource to accelerate the exploration of protein configurations (see figures 2 and 3). However, in nature proteins do not explore the whole exponentially large space of possible configurations in order to fold. In a similar fashion, QFold does not aim to explore all

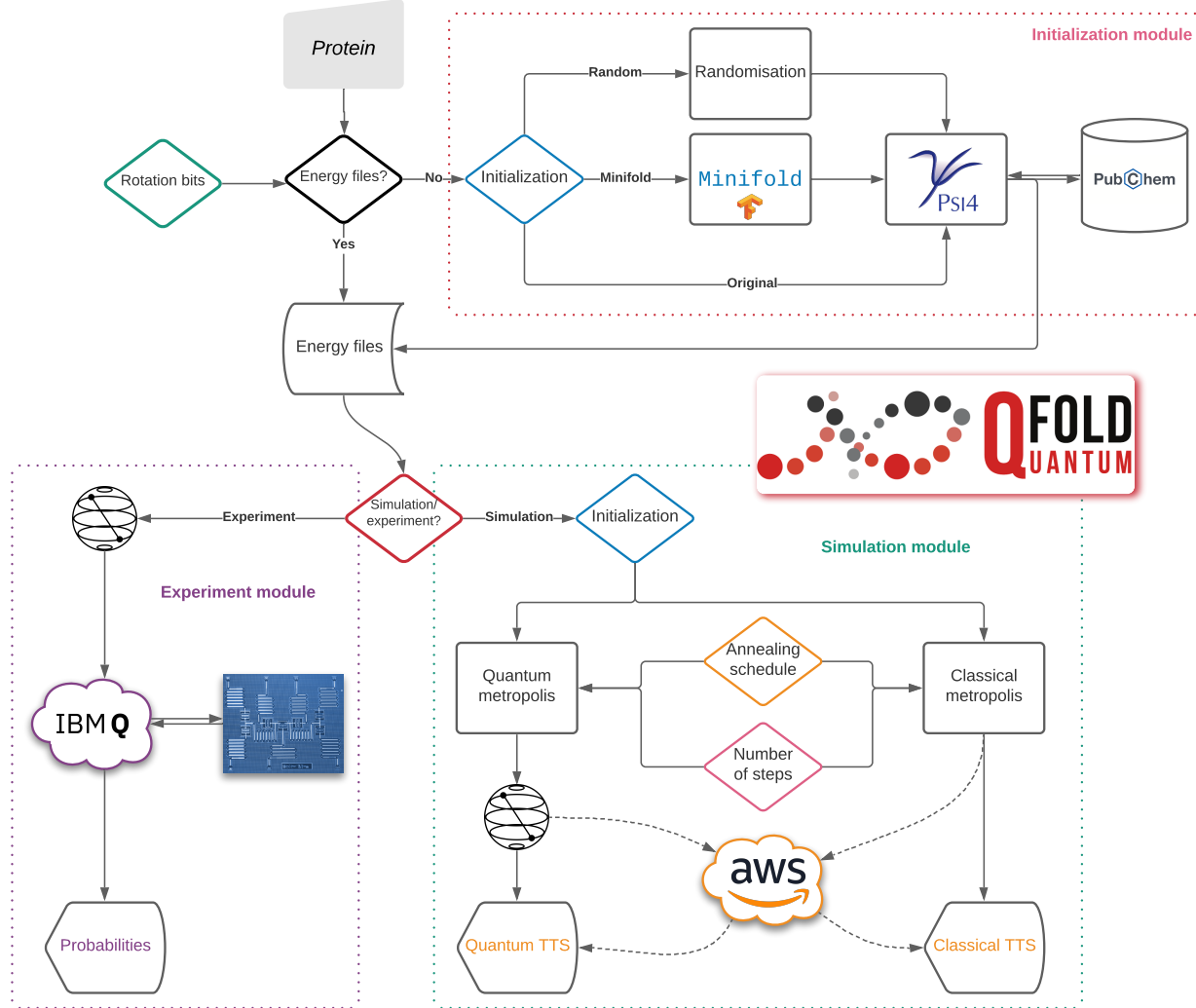


FIG. 3. Flow chart of the QFold algorithm. This figure has to be viewed with the help of figure 2. QFold has several functionalities integrated altogether, that could be summarized in an initialization module, a simulation module, and an experiment module. We denote by diamonds each of the decisions one has to make. The top part constitutes the initialization module, where *Minifold* can be used to get a guess of the correct folding, and *Psi4* uses *PubChem* to calculate the energies of rotations. The bottom half represents the **experiment** or **simulation** algorithms, that output either Probabilities or Quantum/Classical TTS and makes use of *Qiskit*. Different options of the algorithm are represented by diamonds, and more information on them can be found in section III B.

possible configurations, but rather uses a good initialization guess state based on Deep Learning techniques such as AlphaFold. Since such initial point is in principle closer to the actual solution in the real space, we expect it to be most helpful the larger the protein being modelled. In fact, one of the motivations for our work was the fact that adding a Rosetta relaxation at the end of the AlphaFold algorithm was able to slightly improve the results of the AlphaFold algorithm [14]. Notice that a Rosetta relaxation is the way Rosetta calls its classical Metropolis algo-

rithm. Therefore, we expect that improved versions of Rosetta, using in our case quantum walks, could be of help to find an even better solution to the protein folding problem than the one provided by only using AlphaFold.

The AlphaFold initializer starts from the amino acid sequence ( $S$ ), and performs the following procedures:

1. First perform a Multiple Sequence Alignment (MSA) procedure to extract features of the protein already observed in other proteins

whose folding is known.

2. Then, parametrizing the proteins in terms of their backbone torsion angles  $(\phi, \psi)$  (see figure 1), train a residual convolutional neural network to predict distances between amino acids, or as they call them, residues.
3. Train also a separate model that gives a probability distribution for the torsion angle conditional on the protein sequence and its previously analysed MSA features,  $P(\phi, \psi | S, MSA(S))$ . This is done using a 1-dimensional pooling layer that takes the predicted distances between amino acids and outputs different secondary structure such as the  $\alpha$ -helix or the  $\beta$ -sheet [32]. To make the prediction, the algorithm makes use of bins of size  $10^9$ , effectively discretising its prediction.
4. All this information, plus some additional factors extracted from Rosetta, is used to train an effective potential that aims to give smaller energies to the configurations that the model believes to be more likely to happen in nature.

Finally, at inference time one starts from a rough guess using the MSA sequence, and performs gradient descent on the effective potential. One can also perform several attempts with noisy restarts and return the best option. Interestingly enough, the neural network is also able to return an estimation of its uncertainty. Such uncertainty is measured by the parameter  $\kappa$  in the von Mises distribution, and plays the role of the inverse of the variance. The von Mises distribution is the circular analog of the normal distribution, and its use is justified because angles are periodic variables [33].

## B. Classical Metropolis

As we have mentioned in the introduction, a relatively popular approach to perform protein folding has been to use the Metropolis algorithm. The Metropolis algorithm is an algorithm that performs a random walk over the configuration space  $\Omega$ . The configuration space is the abstract space of possible values the torsion angles that a given protein can take. As such, a given state  $i$  is a list of values for such torsion angles. In particular, for computational purposes, we will set that angles can take values from a given set, that is, it will not be a continuous but a discrete distribution. Over such space we can define probability distributions. Furthermore, since those angles will dictate the position of the atoms in the protein, the state  $i$  will also imply an energy level  $E_i$ , due to the interaction of the atoms. In the Rosetta

library, the function that calculates an approximation to such energy is called scoring function.

Starting from a state  $i$ , the Metropolis algorithm proposes a change uniformly at random to one of the configurations,  $j$ , connected to  $i$ . We will call  $T_{ij}$  to the probability of such proposal. Then this change is accepted with probability

$$A_{ij} = \min \left( 1, e^{-\beta(E_j - E_i)} \right), \quad (1)$$

resulting in an overall probability of change  $i \rightarrow j$  at a given step  $\mathcal{W}_{ij} = T_{ij} A_{ij}$ .

Slowly varying  $\beta$  one decreases the probability that steps that increase the energy of the state are accepted, and as a consequence when  $\beta$  is sufficiently large, the end state is a local minima. If this annealing procedure is done sufficiently slowly, one can also ensure that the minima found is the global minima. However, in practice one does not perform this annealing as slowly as required, resorting instead to heuristic restarts of the classical walk, and selecting the best result found by the several different trajectories.

In our implementation we emulate having oracle access to the energies of different configurations. Such oracle in practice is a subroutine that calls the *Psi4* package [34] to calculate the energies of all possible configurations for the torsion angles that we want to explore. We give more detail of our particular implementation in section III B.

## C. Quantum Metropolis

A natural generalisation of the Metropolis algorithm explained in the previous section is the use of quantum walks instead of random walks. The most popular quantum walk for this purpose is Szegedy's [22], that consists of two rotations similar to the rotations performed in Grover's algorithm [35]. Szegedy's quantum walk is defined on a bipartite graph. Given the acceptance probabilities  $\mathcal{W}_{ij} = T_{ij} A_{ij}$ ,  $A_{ij}$  defined in (1), for the transition from state  $i$  to state  $j$ , one defines the unitary

$$U |j\rangle |0\rangle := |j\rangle \sum_{i \in \Omega} \sqrt{\mathcal{W}_{ji}} |i\rangle = |j\rangle |p_j\rangle. \quad (2)$$

Taking

$$R_0 := \mathbf{1} - 2\Pi_0 = \mathbf{1} - 2(\mathbf{1} \otimes |0\rangle \langle 0|) \quad (3)$$

the reflection over the state  $|0\rangle$  in the second subspace, and  $S$  the swap gate that swaps both subspaces, we define the quantum walk step as

$$W := U^\dagger S U R_0 U^\dagger S U R_0. \quad (4)$$

We refer to Appendix A and Fig. 9 for a detailed account on the use of these quantum walks in a similar way to the Grover rotations. For completeness, in Appendix A we review in more detail the theoretical basis of Szegedy quantum walks that leads us to believe that a quantum advantage is possible in our problem.

It is well known that if  $\delta$  is the eigenvalue gap of the classical walk, and  $\Delta$  the phase gap of the quantum walk, then the complexity of the classical walk is  $O(\delta^{-1})$ , the complexity of the quantum algorithm  $O(\Delta^{-1})$ , and the relation between the phase and eigenvalue gap is given by  $\Delta = \Omega(\delta^{1/2})$  [36], offering a potential quantum advantage. Our algorithm aims to explore what is the corresponding efficiency gain in practice.

The quantum Metropolis algorithm that we employ [21] uses a small modification of the Szegedy quantum walk, substituting the bipartite graph by a coin. That is, we will have 3 quantum registers:  $|\cdot\rangle_S$  indicating the current state of the system,  $|\cdot\rangle_M$  that indexes the possible moves one may take, and  $|\cdot\rangle_C$  the coin register. We may also have ancilla registers  $|\cdot\rangle_A$ . The quantum walk step is then

$$\tilde{W} = RV^\dagger B^\dagger FBV. \quad (5)$$

Here  $V$  prepares a superposition over all possible steps one may take in register  $|\cdot\rangle_M$ ,  $B$  rotates the coin qubit  $|\cdot\rangle_C$  to have amplitude of  $|1\rangle_C$  corresponding to the acceptance probability indicated by (1),  $F$  changes the  $|\cdot\rangle_S$  register to the new configuration (conditioned on the value of  $|\cdot\rangle_M$  and  $|\cdot\rangle_C = |1\rangle_C$ ), and  $R$  is a reflection over the state  $|0\rangle_{MCA}$ .

Although other clever options are available [21], here we implement the simplest heuristic algorithm, which consists of implementing  $L$  steps of the quantum walk

$$|\psi(L)\rangle := \tilde{W}_L \dots \tilde{W}_1 |\pi_0\rangle, \quad (6)$$

where  $t = 1, \dots, L$  also defines an annealing schedule, for chosen values of  $\beta(t)$  at each step. More detailed explanation of algorithm [21] can be found in appendix B.

### III. SIMULATIONS, EXPERIMENTS AND RESULTS

#### A. Figures of merit

When looking for a metric to assess the goodness of given solutions to protein folding we have to strike a balance between two important aspects: on the one hand, we want a model that with high probability finds the correct solution. On the other hand,

we would like such procedure to be fast. For example going through all configuration solutions would be quite accurate albeit extremely expensive if not directly impossible.

A natural metric to use in this context is then the Total Time to Solution (TTS) [21] defined as the average expected time it would take the procedure to find the solution if we can repeat the procedure in case of failure:

$$TTS(t) := t \frac{\log(1 - \delta)}{\log(1 - p(t))}. \quad (7)$$

where  $t \in \mathbb{N}$  is the number of quantum/random steps performed in an attempt of the quantum/classical Metropolis algorithm,  $p(t)$  the probability of hitting the right state after those steps in each attempt, and  $\delta$  a target success probability of the algorithm taking into account restarts, that we set to the usual value of 0.9. In any case, since it is a constant, the value of  $TTS(t)$  with other value of  $\delta$  is straightforward to recover. Although one should not expect to be able to calculate  $p(t)$  in the average protein because finding the ground state is already very challenging, for smaller instances it is possible to calculate the  $TTS$  for example executing the algorithm many times and calculating the percentage of them that correctly identifies the lowest energy state. Using quantum resources, the corresponding definition is (B7) from appendix B.

We can see that this metric represents the compromise between longer walks and the corresponding expected increase in probability of success. Using this figure the way we have to compare classical and quantum walks is to compare the minimum values achieved for the  $\min_t TTS(t)$ . Similar metrics have also been defined previously in the literature [37].

On the other hand we would also like mention that there is a small modification of the classical algorithm that could improve its TTS, because we only output the last configuration of the random walk instead of the state with minimum energy found so far, a common choice for example in the Rosetta@Home project. The reason for not having included this modification is because the length of the classical path, 2 to 50 steps, represents a sizable portion of the total space that ranges from 64 to 4096 available positions, whereas that will not be the case for large proteins. We believe that had we run the classical experiments with that modification, we would have introduced a relatively large bias in the results, favouring the classical random walks in the smallest instances of the problem, and therefore likely overestimating the quantum advantage.

For the experiment run in IBM Quantum systems and whose results can be found in section III C 4, the metric we use instead of the TTS is the proba-

bility of measuring the correct answer, and in particular whether we are able to detect small changes in the probability corresponding to the correct solution. Measuring the TTS here would not be interesting due to the high level of noise of the circuit.

## B. Simulation and experimental setup

### 1. Simulations

For the assessment of our algorithm we have built a simulation pipeline that allows to perform a variety of options. The main software libraries used are *Psi4* for the calculation of energies of different configurations in peptides [34], a distilled unofficial version of AlphaFold dubbed *Minifold* [38], and *Qiskit* [39] for the implementation of quantum walks. Simulations were run on personal laptops and small clusters for prototyping, and due to its large computational cost, Amazon Web Services [40] for deploying the complete algorithm and obtaining the results. A scheme of the pipeline of the simulation algorithm can be seen in figure (3).

The initialization procedure takes as input the name of the peptide we want to simulate and uses *Psi4* to download the file of the corresponding molecule from *PubChem* [41], an online repository containing abundant information over many molecules, including atomic positions.

After that, and before executing the quantum and classical walks, the system checks whether an energy file is available, and if not uses *Psi4* to calculate and store all possible energy values of the different rotations of the torsion angles. For the calculation of that energy we choose the relatively common 6-31G atomic orbital basis functions [42], and the procedure of Moller-Plesset to second order [43] as a more accurate and not too expensive alternative to the Hartree-Fock procedure. However, it is also possible to choose any other **basis** or **energy** **method**. Finally, the system performs the corresponding quantum and random walks and returns the minimum TTS found.

In order to evaluate the impact of adding a machine learning module such as AlphaFold at the beginning of the algorithm, we have implemented the initialization option to start from **random** values of the dihedral angles, from the ones returned by **minifold**, or the actual **original** angles that the molecule has, as returned by the *PubChem* library.

On the other hand, to evaluate the potential quantum advantage, we also allow to select the number of bits that specify the discretization of the torsion angles. For example, 1 bit means that angles can take values in  $\{0, \pi\}$ , whereas 2 bits indicate discretiza-

tion in  $\pi/2$  radians. In general, the precision of the angles will be  $2^{1-b}\pi$ , for  $b$  the number of **rotation bits**. Notice that the precision of  $10^9$  of AlphaFold when reporting their angles, that we indicated in section II A, is intermediate between  $b = 5$  and  $b = 6$ . The main idea here is that when we increase  $b$  or the number of angles, the size of the search space becomes larger, and evaluating how the classical and quantum  $\min_t TTS(t)$  grow we may be able to check whether a polynomial quantum advantage exists. The *TTS* can be directly calculated from inferred classical probabilities, if one is executing the classical metropolis or the quantum Metropolis in quantum hardware, or from the amplitudes, if one is running a simulation of the latter. Its specific definition can be seen in equation (7).

Finally, we implemented and used the **experiment** mode, that in contrast to the **simulation** mode explained in previous paragraphs, allows us to run the smallest instances of our problem in actual IBM Q hardware, dipeptides with a single **rotation bit**.

Other choices we have to make involve the value of the parameter  $\beta$  in (1), whether it is fixed or follows some annealing schedule, the number of steps for which the system computes their TTS, or the  $\kappa$  parameter from the von Mises distribution if the initialization is given by *Minifold*. In fact, if the original AlphaFold algorithm were to be used, the  $\kappa$  values returned by AlphaFold could actually be used instead of our default value  $\kappa = 1$ , and furthermore the preparation of the amplitudes corresponding to this probability distribution could be made efficient using the Grover-Rudolph state preparation procedure [44].

Additionally, while *Qiskit* allows to recover the probabilities from the amplitudes, to evaluate the classical walks we have to repeat a certain number of times the procedure to infer the probabilities. This number of repetitions is controlled by a variable named **number iterations**, that we have set to  $500 \times (2^b)^{2n-2}$ , where  $b$  is the **number of bits** and  $n$  the number of amino acids, to reflect that larger spaces require more statistics.

If a non-fixed  $\beta$  is attempted, we have implemented and tested several options for the annealing schedule. The implemented schedules are:

- **Boltzmann** or **logarithmic** implements the famous logarithmic schedule [45]

$$\beta(t) = \beta(1) \log(te) = \beta(1) \log(t) + \beta(1). \quad (8a)$$

Notice that the multiplication of  $t$  times  $e$  is necessary in order to make a fair comparison with the rest of the schedules, so that they all start in  $\beta(1)$ . As a consequence, this is not truly the theoretical schedule required to achieve a quadratic speedup.

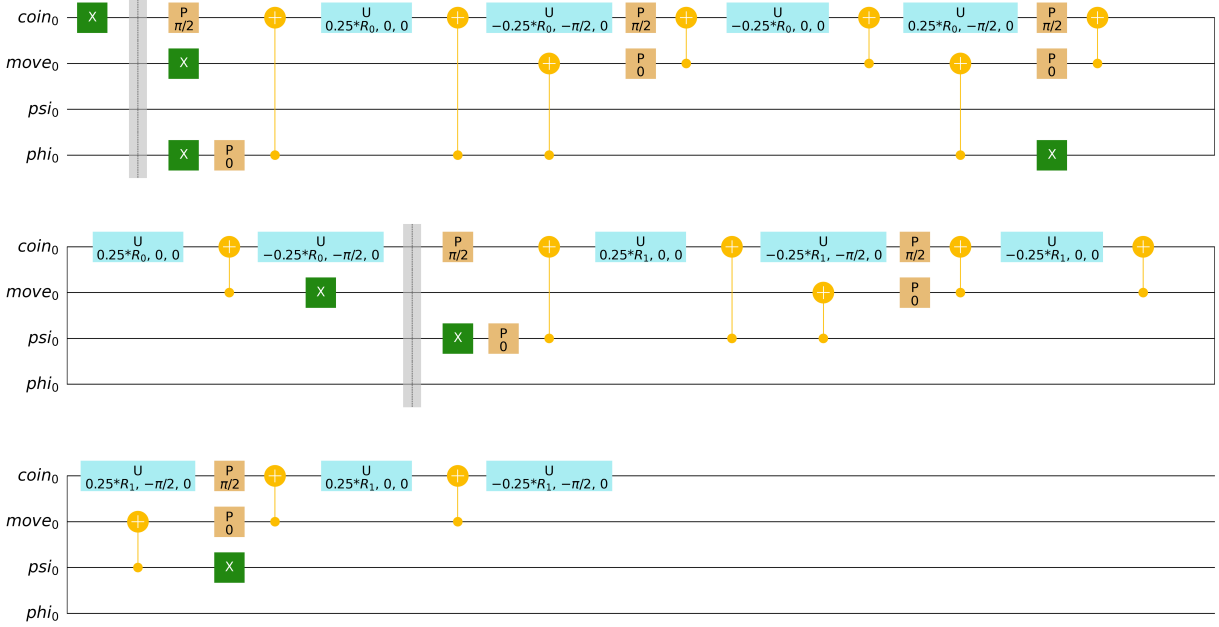


FIG. 4. In section III C 4 we explain a proof of concept experimental realization of the quantum Metropolis algorithm, and this figure represents the implementation of the coin flip subroutine of this hardware-adapted algorithm, whose operator is represented by  $B$  in (5). The circuit has two key simplifications that reduce the depth. The first one is that we first rotate the coin register to  $|1\rangle$  and then we rotate it back to  $|0\rangle$  if the acceptance probability is not 1. This halves the cost, since otherwise one would have to perform 8 multi-controlled rotations (all possible combinations of the control values for registers move,  $\phi$  and  $\psi$ ), and in this case we only perform 4 of them. The second simplification again halves the cost, grouping together rotations with similar values. We empirically see that the rotation values controlled on  $|000\rangle$  and  $|010\rangle$  are very similar, so we group them in rotation  $R_0$ , that implicitly depends on  $\beta$ . Similarly, we group the rotations controlled on  $|001\rangle$  and  $|101\rangle$  in  $R_1$ , also dependent on  $\beta$ . This also has the nice effect of only requiring to control on two out of the three bottom registers, ( $\phi$ ,  $\psi$  and move), transforming CCC- $R_X$  gates in CC- $R_X$ . Separated by the two barriers, from left to right and from top to bottom we can see the implementation of such CC- $R_X$  gates.

- **Cauchy or linear** implements a schedule given by

$$\beta(t) = \beta(1)t. \quad (8b)$$

- **geometric** defines

$$\beta(t) = \beta(1)\alpha^{-t+1}, \quad (8c)$$

where  $\alpha < 1$  is a parameter that we have heuristically set to 0.9.

- And finally **exponential** uses

$$\beta(t) = \beta(1) \exp(\alpha(t-1)^{1/N}), \quad (8d)$$

where  $\alpha$  is again set to 0.9 and  $N$  is the space dimension, which in this case is equal to the number of torsion angles.

For comparison purposes, the value of  $\beta(1)$  chosen has been heuristically optimized to 50.

Our current system has two main limitations depending on the mode it is used. If the aim is to perform a simulation, then the amount of Random Access Memory of the simulator is the main concern. This is why we have simulated, for a fixed value of  $\beta$ :

- Dipeptides with 3 to 5 rotation bits.
- Tripeptides with 2 rotation bits.
- Tetrapeptides with a single rotation bit.

Additionally, dipeptides with 6 bits, tripeptides with 3 bits and tetrapeptides with 2 bits can be simulated for a few steps, but not enough of them to calculate our figure of merit with confidence. If the  $\beta$  value is not fixed but follows some annealing schedule, the requirements are larger, but we can still simulate the same peptides. Further than that, the Random Access Memory requirements for an ideal (classical) simulation of the quantum algorithm become

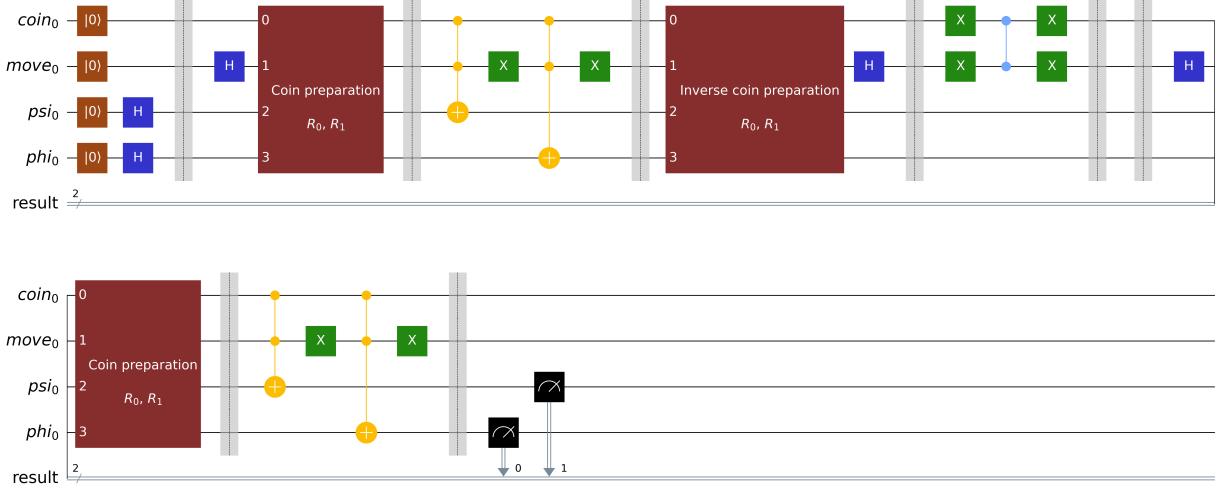


FIG. 5. Implementation of the full quantum Metropolis circuit from section III C 4 implemented in actual quantum hardware, using the coin flip rotation described in figure 4. The steps of the circuit are separated by barriers for a better identification (from left to right, and from top to bottom): first put  $\phi$  and  $\psi$  in superposition. Then, for each of the two steps  $\tilde{W}$  from (5): put the move register (that controls which angle to move) in a superposition, operator  $V$ , and prepare the coin,  $B$ . Then, controlled on the coin being in state  $|1\rangle$  and the move register the corresponding angle, change the value of  $\psi$  (if move =  $|1\rangle$ ) or  $\phi$  (if move =  $|0\rangle$ ), denoted by  $F$ . Then we uncompute the coin,  $B^\dagger$  and the move preparation,  $V^\dagger$ , and perform the phase flip on  $|\text{move}\rangle|\text{coin}\rangle = |00\rangle$  represented by  $R$ . The second quantum walk step proceeds equally (with different value of  $\beta$  and the rotations), but now we do not have to uncompute the move and coin registers before measuring  $\phi$  and  $\psi$  because it is the last step.

quite large. Notice that Qiskit simulator supports 32 qubits at the moment, but our system is more constrained by the depth of the circuit, which can run into millions of gates.

## 2. Experiments

We have also performed experiments in the IBMQ Casablanca processor. In contrast with the previous experiments, due to the low signal to noise ratio in the available quantum hardware, it does not make much sense to directly compare the values of the TTS figure of merit. Instead, the objective here is to be able to show that we can implement a two-step quantum walk (the minimum required to produce interference) and still be able to see an increase in probability associated with the correct state. Since we are heavily constrained in the depth of the quantum circuit we can implement, we experiment only with dipeptides, and with 1 bit of precision in the rotation angles: that is  $\phi$  and  $\psi$  can be either 0 or  $\pi$ .

In this quantum circuit, depicted in figures 4 and 5, we will have 4 qubits, namely  $|\phi\rangle$ ,  $|\psi\rangle$ , a coin qubit, and another indicating what the angle register to update in the next step. Additionally, we always start from the uniform superposition  $|+\rangle_\phi|+\rangle_\psi$ . We

then perform 2 quantum walk steps  $\tilde{W}$  with values of  $\beta$  empirically chosen 0.1 and 1 to have large probabilities of measuring  $|0\rangle_\phi|0\rangle_\psi$ , where we encode the state of minimum energy, the correct state of the dipeptide.

The figures corresponding to the circuit are 4 and 5, the former depicting the coin flip procedure and the latter using it as a subroutine in the circuit as a whole. The coin flip subroutine is the most costly part of the quantum circuit both in this hardware implementation and in the simulations of previous sections too, since it includes multiple multi-controlled rotations of the coin qubit. Perhaps an important remark to make is that this hardware-adapted circuit contains some simplifications in order to minimize the length of the circuit as much as possible, since it will be one of the most important quantities determining the amount of error in the circuit, our limiting factor.

There is one more important precision to be made: since our implementation of the quantum circuit in the IBMQ Casablanca processor has 176 basic gates of depth even after being heavily optimized by *Qiskit* transpiler, we need a way to tell whether what we are measuring is only noise or relevant information survives the noise. Our first attempt to distinguish these two cases was to use the natural technique of zero-noise extrapolation, where additional gates are

Peptides	Precision <code>random</code>	Precision <code>minifold</code>	$b$	quantum min(TTS)	random	quantum min(TTS)	<code>minifold</code>
Dipeptides	0.53	0.53	3	<b>136.25</b>	270.75		
			4	<b>547.95</b>	1137.45		
			5	<b>1426.28</b>	1458.02		
Tripeptides	0.46	<b>0.71</b>	2	499.93		<b>394.49</b>	
Tetrapeptides	0.51	<b>0.79</b>	1	149.80			<b>26.30</b>

TABLE I. Table of average precisions defined in equation (9), and corresponding quantum minimum TTS, defined in equation (7) as the expected number of steps it would take to find the solution using the quantum algorithm, with different initializations.  $b$  denotes the `rotation bits`, and in bold we have indicated which of `minifold` or `random` values are best. The aim of this table is understanding the impact of `minifold` initialization in the quantum min *TTs*, our figure of merit. The two main aspects to notice from the table are that *Minifold* precision grows with the size of the peptide, and that when it is the case that the `minifold` precision is higher, the corresponding quantum min TTS values are lower than their `random` counterparts. This supports the idea that using a smart initial state helps to find the native folding of the protein faster.

added that do not change the theoretical expected value of the circuit, but introduce additional noise [46]. By measuring how the measured probabilities change, one can extrapolate backwards to the theoretical ‘zero noise’ case. Unfortunately, the depth of the circuit is already so large that it does not work: it does not converge or else returns unrealistic results, at least when attempted with the software library *Mitiq* [47].

For this reason we need to find a way out that is only valid because our circuit is parameterised in terms of the angles and the values of  $\beta$ . Additionally we know that if we were to set the value of  $\beta$  to 0, the theoretical result would be 1/4 as there are 4 possible states. As a consequence, our strategy consists of trying to detect changes in the probability when we use  $\beta(t) = (0, 0)$  or  $\beta(t) = (0.1, 1)$ . The notation  $\beta(t)$  denotes the value of  $\beta$  chosen at each of the two steps.

For the experiment, we reserved 3 hours of usage of the IBMQ Casablanca processor, with quantum volume 32. During that time we were able to run 25 so-called ‘jobs’ with  $\beta(t) = (0, 0)$  and 20 ‘jobs’ for 8 arbitrarily chosen dipeptides. Each run consisted of 8192 repetitions of the circuit (which can be seen in figures 4 and 5) and an equal number of measurements, what means that for each dipeptide we run a total of 163840 circuits, and 204800 for  $\beta(t) = (0, 0)$  as a baseline.

As we will see from the results, the main limitation of our experiment is the noise of the system and therefore the depth of the circuit. For this reason we restrict ourselves to a single rotation bit in dipeptides.

### C. Experimental and simulation results

#### 1. Initialization

In this section we analyse the impact of different initialization methods for the posterior use of quantum/classical walks. Although we know that AlphaFold is capable of making a relatively good guess for the correct folding, and therefore it is reasonable to expect AlphaFold’s guess to be close to the optimal folding solution in the conformation space, our aim is to give some additional support to this idea.

As an initializer, we decided to use (and minorly contributed to) *Minifold* because even though it does not achieve the state of the art in the prediction of the angles, it is quite simple and sufficient to illustrate our point. *Minifold* uses a residual network implementation given in Tensorflow and Keras [48, 49]. Perhaps the most important detail of using this model is that because we are trying to predict small peptides, and *Minifold* uses a window of 34 amino acids for its predictions, we had to use padding.

The metrics that we analyse in this case are twofold: in the first place, we would like to see whether *Minifold* achieves a better precision on the angles than random guessing. This is a necessary condition for our use of *Minifold*, or more generally, any smart initialization module, to make sense. We measure the precision as 1 minus the normalized angular distance between the returned value by the initialization module and the actual value we get from *PubChem* (see figures 1 and 2):

$$p = 1 - \frac{d(\alpha, \tilde{\alpha})}{\pi}, \quad (9)$$

where  $\tilde{\alpha}$  is the estimated angle (either  $\phi$  or  $\psi$ ) given by *Minifold* or chosen at random,  $\alpha$  is the true value calculated from the output of *Psi4* and *PubChem*, and  $d$  denotes the angular distance. Since we have

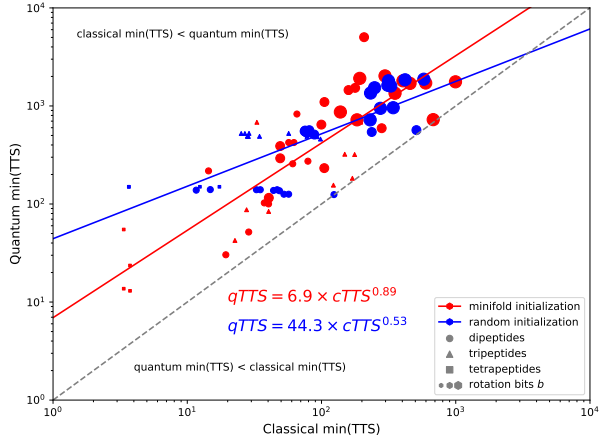


FIG. 6. Comparison of the Classical and Quantum minimum TTS achieved for the simulation of the quantum Metropolis algorithm with  $\beta = 10^3$ , for 10 dipeptides (with **rotation bits**  $b = 3, 4, 5$ ), 10 tripeptides ( $b = 2$ ) and 4 tetrapeptides ( $b = 1$ ), also showing the different initialization options (**random** or **minifold**), and the best fit lines. In dashed grey line we separate the space where the Quantum TTS is smaller than the Classical TTS. The key aspect to notice in this graph is that although for smaller instances the quantum algorithm does not seem to match or beat the times achieved by the classical Metropolis, due to the exponent being smaller than one (either 0.89 or 0.53 for **minifold** or **random** respectively) for average size proteins we can expect the quantum advantage to be dominant and make the quantum Metropolis more useful than its classical counterpart. In section III C 2 we discuss further details and explain why the **random** initialization exponent seems more favourable than the **minifold** exponent.

normalized it, the **random** initialization gets a theoretical average precision of 0.5. In table I there is a summary comparing the average precision results of **minifold** and **random** initialization broken down by the protein and bits. The dipeptide results show that due to the small size of the peptide, **minifold** has barely a better precision than just random. However, this situation improves for tripeptides and tetrapeptides, getting a better precision, and as a consequence, lower TTS values.

If **Minifold** having a greater precision in the angles than random guessing was a precondition for our analysis to make sense, the actual metric we are interested in is whether it has some impact reducing the TTS metric. Otherwise we could avoid using an initialization module altogether. First of all we were not expecting an actual reduction of the exponent due to the use of **minifold** initialization as much as multiplicative TTS reduction prefactors. However, in figure 6 the exponent of **random** initialization model is smaller than the one correspond-

ing to the **minifold** initialization in the fit. While this may seem to indicate that our initialization is in fact harmful to the convergence of the quantum algorithm, in fact the explanation is quite the opposite: for the smaller instances of the problem, and very specially in the case of **random** initialization, the minimum TTS value is achieved for  $t = 2$  as can be seen from the two horizontal structures formed by the blue points in the figure, meaning that in such cases only using the **minifold** initialization the quantum algorithm is able to profit from the incipient quantum advantage. This effect disappears for larger instances of the problem, but while for **random** initialization there is a penalisation of the TTS in the smallest problems (thus lowering the exponent), the **minifold** initialization is capable of correcting for this effect, lowering the TTS of smaller instances of the problem and, as a bonus, rising the exponent. We are therefore inclined to believe that the **minifold** exponent more accurately represents the true asymptotic exponent of the algorithm for this problem. In conclusion, while the small size of our experiments does not allow us to see the benefits of using a smart initialization, they have been important to get a calibrated estimate of the actual quantum advantage, and we can also see that it helps reduce the TTS cost both in the classical and quantum algorithm, which nicely fits the intuition that being closer-than-random to the solution helps to find the solution faster.

## 2. Fixed $\beta$

We now discuss whether we are able to observe a quantum advantage in the TTS, our figure of merit. We will again be discussing the results given in figure 6, for it represents the best fit to the classical vs quantum TTS, and therefore accurately depicts the expected quantum advantage: we can see that the slopes separated for the different initialization options are 0.89 for the **minifold** initialization and 0.53 for the **random** initialization. As a consequence, we can see that if these trends are sustained with larger proteins, there is a polynomial advantage.

As we have seen, figure 6 points towards a quantum advantage. The final question we would therefore like to answer, is what does this advantage mean for the modelling of large enough proteins. For that, we only need one additional ingredient, which is how the expected classical  $\min TTS$  scales with the size of the configuration of the problem. Our data in this respect is even more restricted because we only have access to configuration spaces of 64, 256 and 1024 positions. Therefore we are making a regression to only three points, but could give us nev-

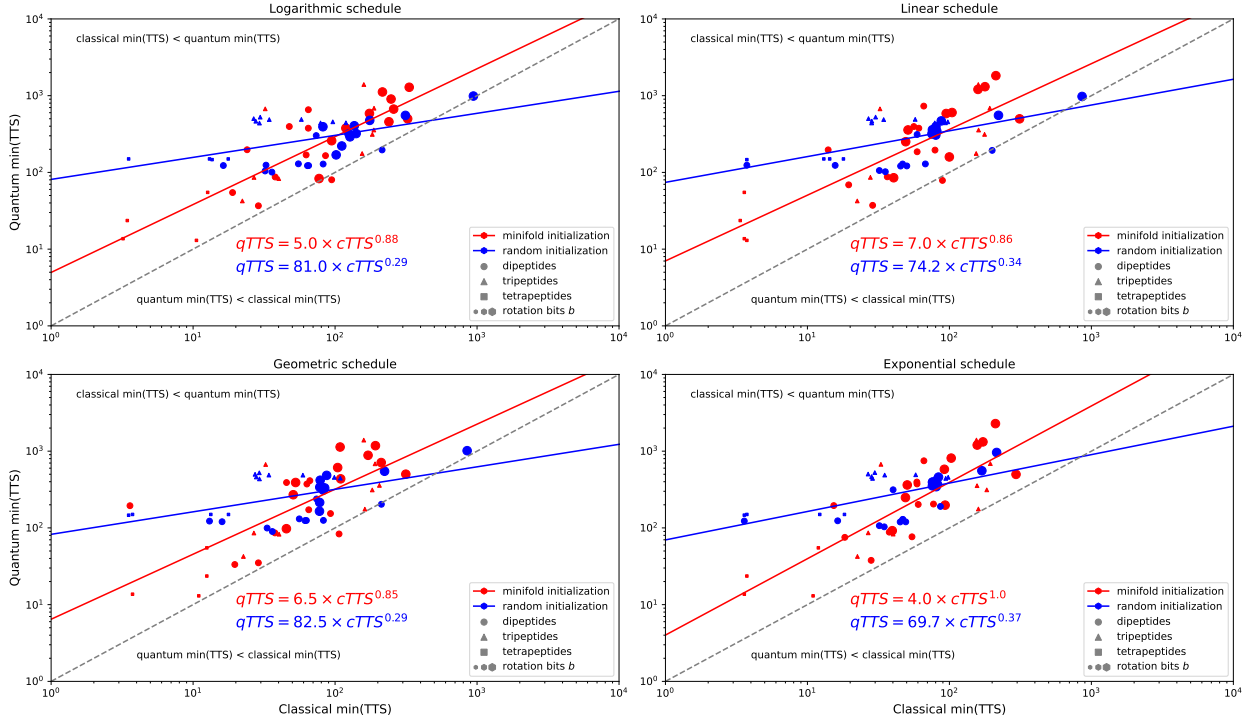


FIG. 7. Comparison of the Classical and Quantum minimum TTS achieved for the same peptides as those in figure 6, except that due to computational cost we do not include dipeptides with 5 rotation bits. This figure corresponds to section III C3, and shows the different initialization options (random or minifold) and annealing schedules (Boltzmann/logarithmic, Cauchy/linear, geometric and exponential), and the best fit lines. In dashed grey line we depict the diagonal. The corresponding fit exponents are given in table II, where we can see that in three out of the four cases using an annealing schedule increases the quantum advantage. On the other hand, using an exponential schedule does not seem to give but a tiny advantage when used with a minifold initialization.

ertheless some hints of whether our technique, the use of quantum Metropolis algorithm, will be helpful to solve the tridimensional structure of proteins given a large enough and fault tolerant quantum computer. The regression exponent of a  $\log(\text{size})$  vs  $\log(\text{classical min TTS})$  fit using both random and minifold initializations is  $r = 0.88$ , that should not be confused with those in figure 6.

Let us take, for the sake of giving an example, an average 250 amino acids protein, which has approximately 500 angles to fix. If we use  $b = 6$  bits to specify such angles as might be done in a realistic setting, the classical  $\min_t TTS$  would be  $\approx (2^b)^{2 \times 250 \times r} = (2^6)^{500 \times 0.88}$ . The quantum  $\min_t TTS$ , on the other hand, will be such number to the corresponding exponent of figure 6, that we will call  $e_m = 0.89$  and  $e_r = 0.53$  for minifold and random. This will translate to a speedup factor of between  $\approx 10^{87}$  and  $10^{373}$ , although the latter represents an upper bound and the former is probably closer to the actual value. This reveals that even if we take into account the slowdown due to error correction and other factors in quantum com-

puting, the use of the quantum Metropolis seems very powerful and competitive. And this conclusion is robust: if we took the quantum advantage exponent to be just  $e = 0.95$  and the growth of the TTS with the size of the space an extremely conservative  $r = 0.5$ , the quantum speedup before factoring in the operating frequency of the computer will still be a factor of  $\approx 10^{22}$ . Larger proteins, which exist in nature, will exhibit even larger speedups in the TTS, the expected time it would take to find the native structure.

### 3. Annealing schedules and variable $\beta$

In the previous section we analysed what quantum advantage could be expected when using a fixed  $\beta$  schedule, resulting in a *pure quantum walk* with several steps. However, Metropolis algorithms are rarely used in practice with a fixed  $\beta$ , since at the beginning of the algorithm one would like to favour exploration, requiring a low  $\beta$  value, and at the end one would like to focus mostly on exploitation, that

Fit exponents		
Schedule	Random init.	Minifold init.
Fixed $\beta$	0.53	0.89
Logarithmic	0.29	0.88
Linear	0.34	0.86
Exponential	0.37	1.00
Geometric	0.29	0.85

TABLE II. Table of scaling exponents for different annealing schedules and initialization options. The peptides are the same, except that for fixed  $\beta$  we have also included dipeptides with 5 bits of precision, what is costly for the rest of schedules. For fixed  $\beta$ , the value heuristically chosen was  $\beta = 1000$ , while the initial  $\beta$  value in each of the schedules, defined in (8), is  $\beta(1) = 50$ .

is achieved with a high  $\beta$  value. It can be seen that this necessity is linked to the well known exploration-exploitation trade-off in Machine Learning and more generally in Optimization [50].

The annealing schedule with the strongest theoretical background is usually called the inhomogeneous algorithm, and it is known because one can prove that the algorithm will converge to the global minimum value of the energy with probability 1, albeit generally too slowly (section 3.2 [51]). Its implementation is conceptually similar to the Boltzmann or logarithmic schedule that we use, but with a different prefactor [51].

Therefore, the question we would like to answer in this section is what happens when we use our quantum Metropolis algorithm outside of the equilibrium, that is, when we use a schedule that changes faster than the theoretical inhomogeneous algorithm. For this task, several optimization schedules have been proposed, of which we have implemented and tested four different options whose mathematical formulation can be seen in (8).

Our conclusions from figure 7 and table II are that using a variable schedule, the quantum advantage can be made larger than that of the fixed the temperature algorithm. However, not all cases give the same advantage, with the **exponential** schedule giving practically none, and the **geometric** schedule explained in section 5.2 of [51] being the most promising, with an exponent of 0.85 if **minifold** initialization is used. **Linear** and **logarithmic** schedules lie in between.

Lastly, large differences in the exponents exist depending on the initialization criteria used, although the same argument on why this is the case given in section III C 2 applies here too. In consequence, a more detailed analysis should be carried out in future work. However, from figures 6 and 7 we can see that the decrease in the expected TTS value when using a **minifold** initialization is reflected in the corresponding prefactors, smaller and more favourable.

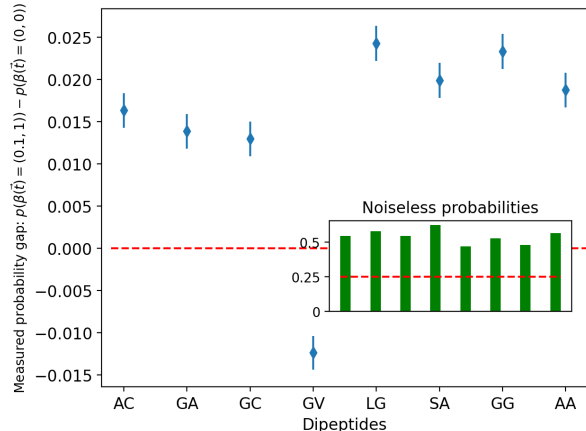


FIG. 8. Results from hardware measurements corresponding to the experimental realization of the quantum Metropolis described in section III C 4 and the circuit depicted in figures 4 and 5. For each dipeptide we perform a student t-test to check whether the average success probabilities for  $\beta(t) = (0, 0)$  and  $\beta(t) = (0.1, 1)$  are actually different [52]. The largest p-value measured in all 8 cases is  $3.94 \cdot 10^{-18}$ , indicating that in all cases the difference is significant. For each of the eight dipeptides we run 163840 times the circuit, and for the baseline 204800 times.

#### 4. Experiments in IBMQ Casablanca

After having analysed the potential quantum advantage in simulation, we would also like to implement the quantum Metropolis in IBM Q Casablanca processor. The circuit we have implemented is made of two quantum walk operators, the minimum required to cause interference, in the smallest instance of our problem: dipeptides with a single rotation bit, thus allowing for angles of 0 and  $\pi$ .

The corresponding implementation of the circuit, which was run in IBMQ Casablanca processor, is depicted in figures 4 and 5. An important detail of our implementation of this quantum Metropolis algorithm is that in order to be able to see more than noise we have needed to perform simplifications that benefit from the particular structure of the problem. This allows us to minimize the depth of the circuit, that strongly influences the noise, the limiting figure of our experiment.

In fact, both due to the high level of noise of the circuit, and the minimal size of the problem we are trying to solve, which only has 4 possible states to search from, in this experiment it does not make sense to use the Total Time to Solution as a figure of merit. Rather, we are only interested in seeing if the quantum circuit is sensitive to the underlying probabilities, which depend on the chosen  $\beta$  value. As we

discussed in section III B 2, for  $\beta = 0$  all states are equiprobable whereas for higher  $\beta$  values the probability of the target state is higher, and our experiment aims to see this difference of probability in practice.

The depicted circuit, with values of  $\beta(\mathbf{t}) = (0, 0)$  and  $\beta(\mathbf{t}) = (0.1, 1)$  was run as explained in the section III B 2 for several hundred thousand times for each dipeptide to be able to certify that our measurements do not correspond to pure noise. The results of such probability differences are depicted in figure 8, and they are highly significant as indicated by the low p-value achieved in all cases, smaller or equal to  $3.94 \cdot 10^{-18}$ , in the corresponding student t-test of the underlying binomial distribution. Such binomial distribution corresponds to returning value 1 when the measurement correctly identifies the minimum-energy state which is encoded in  $|00\rangle$ , and 0 when it does not.

It can also be seen that in seven out of the eight cases tested, the quantum Metropolis algorithm points in the right direction of increased success probability. This gives us confidence that we are measuring a small amount of quantum effects. The outlier, glycylvaline, is surprising because is the dipeptide that in the simulation shows the greatest theoretical probability of measuring  $|00\rangle$ , and at the same time is the dipeptide with the largest p-value, although still very significant. We can only hypothesise that this is due to some experimental imperfection.

#### IV. CONCLUSIONS AND OUTLOOK

We have studied how quantum computing might complement modern machine learning techniques to predict the folding of the proteins. For that, we have introduced QFold, an algorithm that implements a quantum Metropolis algorithm using as a starting guess the output of a machine learning algorithm, that in our case is a simplified implementation of AlphaFold algorithm named Minifold, but that could in fact be substituted by any initialization module that uses future improvement of such deep learning techniques.

An important feature of QFold is that it is a realistic description of the protein folding, meaning that the description of the folded structure relies on the actual torsion angles that describe the final conformation of the protein. This is realised by the number of bits  $b$  used to fix the precision of those angles, for which a moderate value of  $b = 5$  or  $b = 6$  would be as accurate as the original AlphaFold. This is in sharp contrast with the rigid lattice models used to approximate protein folding in the majority of

quantum computing algorithmic proposals for protein folding. Although in our current simulations presented in this work the range of the precision is limited by the resources of the classical simulation, nothing prevents QFold from reaching a realistic accurate precision once a fully fledged quantum computer is at our disposal, since our formulation is fully scalable within a fault-tolerant scenario.

The quantum Metropolis algorithm itself relies on the construction of a coined version of Szegedy quantum walk [21], and we use the Total Time to Solution defined in (7), as a figure of merit. Our construction of this quantum Metropolis algorithm represents the first main contribution of our work, as it represents a scalable and realistic algorithm for protein folding that in contrast to previous proposals, does not rely on simplified lattice models.

The second main contribution is an analysis of the expected quantum advantage in protein folding, that although moderate in the scaling exponent with the Minifold initialization, could represent a large difference in the expected physical time needed to find the minimal energy configuration in proteins of average size due to the exponential nature of this combinatorial problem. This quantum advantage analysis is also performed for different realistic annealing schedules, indicating that the out-of-equilibrium quantum Metropolis algorithms can show a similar quantum advantage, and can even improve the advantage shown for the fixed beta case, as can be seen from table II. The third contribution is a proof-of-concept small implementation of our algorithm in actual quantum software.

Our results for the computation of protein folding provide further support to the development of classical simulations of quantum hardware. A clear message from our simulations is that it is worthwhile developing quantum software and classical simulations of ideal quantum computers in order to confirm that certain quantum algorithms provide a realistic quantum advantage. Some of the quantum algorithms that must be assessed in realistic conditions are those based on quantum walks like quantum Metropolis variants with fast annealing schedule. For them, the complexity scales as  $O(\delta^{-a})$ ,  $\delta$  the eigenvalue gap, and  $a > 0$  dependent on the specific application and realization of the quantum Metropolis. This is in contrast with *pure quantum walks*, where the classical complexity scales as  $O(\delta^{-1})$  and the quantum complexity as  $O(\delta^{-1/2})$ , as can be seen in appendix B. However, it would be naïve to consider this quadratic quantum advantage as an achievable and useful one in problems similar to ours. Instead, one should aim to compare quantum algorithms with the classical ones used in practice, where heuristic annealing schedules are used

instead. As a consequence, finding out the precise values of the corresponding exponent is of great importance since it is a measure of the quantum advantage. For this reason, not all efforts should be devoted to finding a quantum advantage solely with noisy ‘baby quantum computers’, like NISQ devices, but also to continue investigating the real possibilities of universal quantum computers when they become available.

An unknown that is worth addressing is whether the new software for protein folding coming out of the CASP competition [13] will remain in the public domain or else, will go proprietary. This is especially important since some the most powerful tools used by that modern software rely on deep learning that has to be trained. It so happens that the protein databases used for that training are of public domain. They are the result of many years of collaborative work among many research institutions that are funded publicly. Our results point towards the possibility of using an open public software like *Qiskit* [39], *Psi4* [34] and ‘community’ implementations of the AlphaFold algorithm [14] of which *Minifold* [38] is an example, to compensate the power of commercial software for protein folding.

We would also like to point out that despite the great advances achieved by the new classical methods in the latest editions of the CASP competition [13], there is still huge room for improvement and there are many gaps in the problem of protein folding that await to be filled. These include understanding protein-protein and protein-ligand interactions, the real time folding evolution to the equilibrium configuration, the dark proteome, proteins with dynamical configurations like the intrinsically disordered proteins (IDP) and so on and so forth. Crucially, we believe that the current limitations of the training data sets, which are biased towards easily to be crystallized proteins, puts constraints on what can be achieved using only deep learning techniques. Our present research is an attempt to explore techniques that address these limitations.

Future improvements of our work include primarily a refinement of our experimentally found quantum advantage, with peptides of larger size, and a more accurate comparative analysis of the precise quantum advantage that can be found with each annealing schedule. Such research would be valuable because it is an important decision to be made when deploying these optimization algorithms in practice, and no research of this question has been carried out to the best of our knowledge.

Additionally, we also believe further work should be conducted in clarifying whether asymptotically one should expect either of the initialization modes to be polynomially faster finding the ground state.

Similar quantum Metropolis algorithms could be used in a variety of domains, and as such a detailed analysis, both theoretical and experimental, of the expected quantum advantage in each case seems desirable.

## V. ACKNOWLEDGEMENTS

P.A.M.C and R.C contributed equally to this work. We would like to thank kind advice from Jaime Sevilla on von Mises distributions and statistical t-tests, Alvaro Martínez del Pozo and Antonio Rey on protein folding, Andrew W. Senior on minor details of his AlphaFold article, Carmen Recio, Juan Gómez, Juan Cruz Benito, Kevin Kruslich and Maddy Todd on the usage of Qiskit, and Jessica Lemieux and the late David Poulin on aspects of the quantum Metropolis algorithm. We also want to thank IBM Quantum Research for allowing us to use their quantum processors under the Research program. We also thank Quasar Science for facilitating the access to the AWS resources. We acknowledge financial support from the Spanish MINECO grants MINECO/FEDER Projects FIS 2017-91460-EXP, PGC2018-099169-B-I00 FIS-2018 and from CAM/FEDER Project No. S2018/TCS-4342 (QUITEMAD-CM). The research of M.A.M.-D. has been partially supported by the U.S. Army Research Office through Grant No. W911NF-14-1-0103. P. A. M. C. thanks the support of a MECD grant FPU17/03620, and R.C. the support of a CAM grant IND2019/TIC17146.

## Appendix A: Szegedy quantum walks

In order to explain what are Quantum Walks, we need to introduce Markov Chain. Given a configuration space  $\Omega$ , a Markov Chain is a stochastic model over  $\Omega$ , with transition matrix  $\mathcal{W}_{ij}$ , that specifies the probability of transition that does not depend on previous states but only on the present one. Random walks are the process of moving across  $\Omega$  according to  $\mathcal{W}_{ij}$ .

Quantum walks are the quantum equivalent of random walks [53]. The most famous and used quantum walks are those defined by Ambainis [54] and Szegedy [22], although several posterior generalisations and improvements have been developed such as those in [36]. Quantum walks often achieve a quadratic advantage in the hitting time of a target state with respect to the spectral gap, defined below, and are widely used in several other algorithms [55–57], as we shall see.

Szegedy quantum walks are not usually defined

using a coin, but rather on a bipartite walk. This implies duplicating the Hilbert space, and defining the unitary

$$U |j\rangle |0\rangle := |j\rangle \sum_{i \in \Omega} \sqrt{\mathcal{W}_{ji}} |i\rangle = |j\rangle |p_j\rangle \quad (\text{A1a})$$

and also the closely related

$$V |0\rangle |i\rangle := \sum_{j \in \Omega} \sqrt{\mathcal{W}_{ij}} |j\rangle |i\rangle = |p_i\rangle |i\rangle. \quad (\text{A1b})$$

$\mathcal{W}_{ij}$  must be understood as the probability that state  $|i\rangle$  transitions to state  $|j\rangle$ . We can check that these operators fulfil that  $SU = VS$ , for  $S$  the Swap operation between the first and second Hilbert subspace. The cost of applying  $U$  is usually called (quantum) update cost. Define also the subspaces

$$\mathcal{A} := \text{span}\{|j\rangle |0\rangle : j \in \Omega\} \quad (\text{A2a})$$

and

$$\mathcal{B} := U^\dagger SU\mathcal{A} = U^\dagger VS\mathcal{A}. \quad (\text{A2b})$$

Having defined  $U$  and  $V$ , we can define  $M := U^\dagger VS$ , a matrix with entries valued  $\langle i, 0 | U^\dagger VS | j, 0 \rangle = \sqrt{\mathcal{W}_{ji}} \sqrt{\mathcal{W}_{ij}} = \sqrt{\pi_i / \pi_j} \mathcal{W}_{ij}$ , the last equality thanks to the detailed balance equation [58]. In fact, in matrix terms it is usually written  $M = D_\pi^{-1/2} \mathcal{W} D_\pi^{1/2}$  where we have written  $D_\pi$  to indicate the diagonal matrix with the entries of the equilibrium state-vector of probabilities,  $\pi$ . This implies that  $\mathcal{W}$  and  $M$  have the same spectrum  $\lambda_0 = 1 \geq \dots \geq \lambda_{d-1} \geq 0$ , as the matrix  $\mathcal{W}$  is positive definite,  $p^T \mathcal{W} p \in [0, 1]$ , and of size  $d$ . The corresponding eigenstates are  $|\phi_j\rangle |0\rangle$ , and phases  $\varphi_j = \arccos \lambda_j$ . In particular  $|\phi_0\rangle = \sum_i \sqrt{\pi_i} |i\rangle$ , is the equilibrium distribution.

We can also define the projectors around  $\mathcal{A}$  and  $\mathcal{B}$  as  $\Pi_{\mathcal{A}}$  and  $\Pi_{\mathcal{B}}$

$$\Pi_{\mathcal{A}} := (\mathbf{1} \otimes |0\rangle \langle 0|), \quad (\text{A3a})$$

$$\Pi_{\mathcal{B}} := U^\dagger VS(\mathbf{1} \otimes |0\rangle \langle 0|)SV^\dagger U \quad (\text{A3b})$$

with their corresponding rotations

$$R_{\mathcal{A}} = 2\Pi_{\mathcal{A}} - \mathbf{1}, \quad (\text{A4a})$$

$$R_{\mathcal{B}} = 2\Pi_{\mathcal{B}} - \mathbf{1}. \quad (\text{A4b})$$

Using this rotation we further define a quantum walk step as we did in the main text equation (4),

$$W = R_{\mathcal{B}} R_{\mathcal{A}} = U^\dagger S U R_{\mathcal{A}} U^\dagger S U R_{\mathcal{A}}. \quad (\text{A5})$$

Using the previous expressions we can state, using  $\Pi_{\mathcal{A}} |\phi_j\rangle |0\rangle = |\phi_j\rangle |0\rangle$

$$\Pi_{\mathcal{A}} U^\dagger VS |\phi_j\rangle |0\rangle = \cos \varphi_j |\phi_j\rangle |0\rangle, \quad (\text{A6a})$$

and

$$\Pi_{\mathcal{B}} |\phi_j\rangle |0\rangle = U^\dagger VS \cos \varphi_j |\phi_j\rangle |0\rangle. \quad (\text{A6b})$$

(A6b) is true because (supplementary material [20]),

$$\Pi_{\mathcal{A}} U^\dagger VS \Pi_{\mathcal{A}} = \Pi_{\mathcal{A}} S V^\dagger U \Pi_{\mathcal{A}} \quad (\text{A7})$$

due to

$$\begin{aligned} \langle \phi_j, 0 | \Pi_{\mathcal{A}} U^\dagger VS \Pi_{\mathcal{A}} | \phi_j, 0 \rangle &= \lambda_j \\ &= \lambda_j^\dagger = \langle \phi_j, 0 | \Pi_{\mathcal{A}} S V^\dagger U \Pi_{\mathcal{A}} | \phi_j, 0 \rangle. \end{aligned} \quad (\text{A8})$$

Thus  $W$  will preserve the subspace spanned by  $\{|\phi_j\rangle |0\rangle, U^\dagger VS |\phi_j\rangle |0\rangle\}$ , which is invariant under  $\Pi_{\mathcal{A}}$  and  $\Pi_{\mathcal{B}}$ ; mirroring the situation in the Grover algorithm [35]. Also, as a consequence of the previous, and of the fact that in  $\mathcal{A} + \mathcal{B}$  operator  $W$  has eigenvalues  $e^{2i\varphi_j}$  [22, 36], in such subspace the operator  $W$  can be written as a block diagonal operator with matrices

$$w_j = \begin{pmatrix} \cos(2\varphi_j) & -\sin(2\varphi_j) \\ \sin(2\varphi_j) & \cos(2\varphi_j) \end{pmatrix}. \quad (\text{A9})$$

Finally, notice that the eigenvalue gap of  $\mathcal{W}$  is defined as  $\delta = 1 - \lambda_1$ , and in general the hitting time of a classical walk will grow like  $O(\delta^{-1})$  (Proposition 1 of [36]). On the other hand, the hitting time of the Quantum Walk will scale like  $O(\Delta^{-1})$  (Theorem 6 of [36]), where  $\Delta := 2\varphi_1$ . But  $\Delta \geq 2\sqrt{1 - |\lambda_1|^2} \geq 2\sqrt{\delta}$ , so  $\Delta = \Omega(\delta^{1/2})$ . In fact, writing  $\delta = 1 - \lambda_1 = 1 - \cos \varphi_1$ , and expanding in Taylor series  $\cos \varphi_1 = 1 - \frac{\varphi_1^2}{2} + \frac{\varphi_1^4}{24} + O(\varphi_1^6)$ , we can see that

$$\frac{\varphi_1^2}{2} \geq 1 - \cos \varphi_1 \geq \frac{\varphi_1^2}{2} - \frac{\varphi_1^4}{24}. \quad (\text{A10})$$

Using the definitions of  $\delta$  and  $\Delta$  and the fact that  $\varphi_1 \in (0, \pi/2)$ , it is immediate

$$\begin{aligned} \frac{\Delta^2}{8} \geq \delta &\geq \frac{\Delta^2}{8} - \frac{\Delta^4}{2^4 \cdot 24} = \frac{\Delta^2}{8} \left(1 - \frac{\Delta^2}{2 \cdot 24}\right) \\ &\geq \frac{\Delta^2}{8} \left(1 - \frac{\pi^2}{2 \cdot 24}\right). \end{aligned} \quad (\text{A11})$$

Consequently,  $\Delta = \Theta(\delta^{1/2})$ , and this is the reason why Quantum Walks are quadratically faster than their classical counterparts.

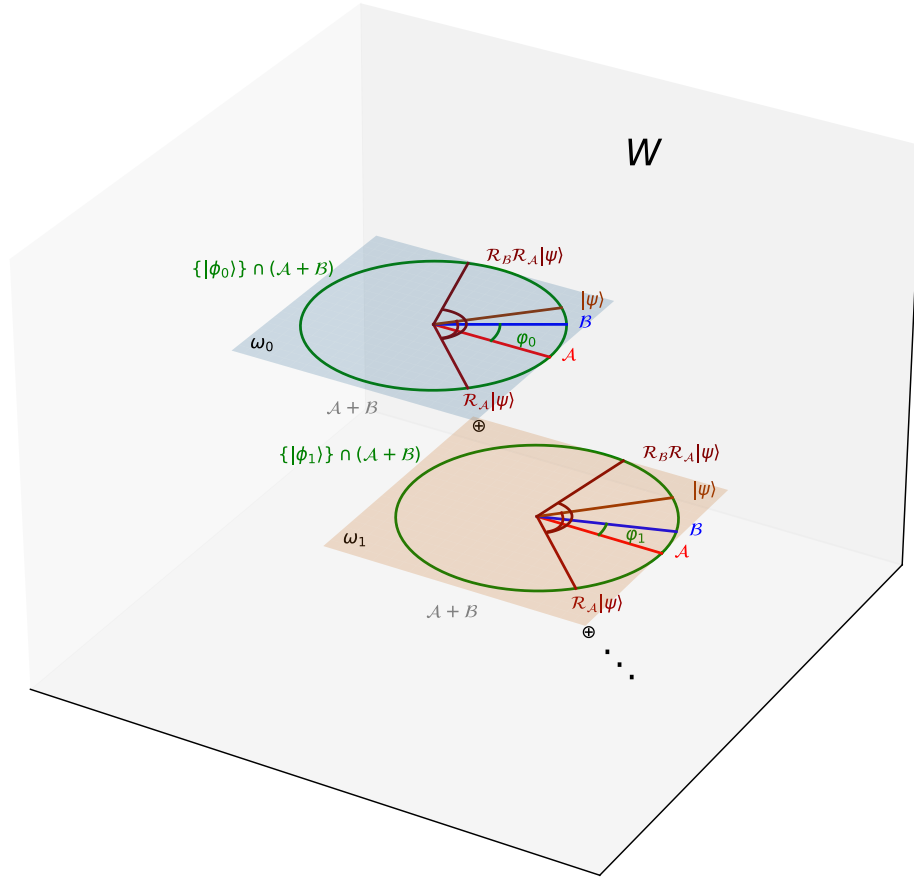


FIG. 9. Geometrical visualization of a quantum walk operator  $W$  of Szegedy type.  $W$  performs a series of rotations that in the subspace  $\mathcal{A} + \mathcal{B}$ , defined in (A2) with their corresponding rotation operators (A4), may be written as a block diagonal matrix, where each block is a 2-dimensional rotation  $\omega_j = R(2\varphi_j)$  given by (A9). This figure represents the direct sum of Grover-like rotations in the subspace spanned by  $\mathcal{A} + \mathcal{B}$ , and therefore  $W$ . This quantum walk operator represents equation (4) from section II C.

### Appendix B: Mathematical description of the out-of-equilibrium quantum Metropolis algorithm

In the appendix A we have reviewed the Szegedy quantum walk. In this appendix, we present a quantum Metropolis-Hastings algorithm based on the use of Szegedy walks.

The objective of the Metropolis-Hastings algorithm is sampling from the Gibbs distribution  $\rho^\beta = |\pi^\beta\rangle\langle\pi^\beta| = Z^{-1}(\beta)\sum_{\phi\in\Omega}e^{-\beta E(\phi)}|\phi\rangle\langle\phi|$ , where  $E(\phi)$  is the energy of a given configuration of angles of the molecule,  $\beta$  plays the role of the inverse of a temperature that will be lowered during the process, and  $Z(\beta) = \sum_{\phi\in\Omega}e^{-\beta E(\phi)}$  a normalization factor.  $\Omega$  represents the configuration space, in our case the possible values the torsion angles may take. One can immediately notice that if  $\beta$  is sufficiently large only the configurations with the lowest possible energy

will appear in when sampling from that state, with high probability. Thus, we wish to prepare one such state to be able find the configuration with the lowest energy, in our case the folded state of the protein in nature.

One way to construct such distribution  $\pi^\beta$  is to create a rapidly mixing Markov Chain that has as equilibrium distribution  $\pi^\beta$ . Such Markov Chain is characterized, at a given  $\beta$ , by a transition matrix  $\mathcal{W}$  that induces a random walk over the possible states. That is,  $\mathcal{W}$  maps a given distribution  $p$  to another  $p' = \mathcal{W}p$ . Let us introduce some useful definitions: an aperiodic walk is called *irreducible* if any state in  $\Omega$  can be accessed from any other state in  $\Omega$ , although not necessarily in a single step. Additionally, we will say that a walk is *reversible* when it fulfills the detailed balance condition

$$\mathcal{W}_{j,i}^\beta \pi_i^\beta = \mathcal{W}_{i,j}^\beta \pi_j^\beta. \quad (\text{B1})$$

Metropolis-Hastings algorithm uses the following transition matrix

$$\mathcal{W}_{ij} = \begin{cases} T_{ij} A_{ij}, & \text{if } i \neq j \\ 1 - \sum_{k \neq j} T_{kj} A_{kj}, & \text{if } i = j, \end{cases} \quad (\text{B2})$$

where, as given in the main text equation (1),

$$A_{ij} = \min \left( 1, e^{-\beta(E_i - E_j)} \right), \quad (\text{B3})$$

and

$$T_{ij} = \begin{cases} \frac{1}{N} & \text{there is a move connecting } j \text{ to } i \\ 0, & \text{else,} \end{cases} \quad (\text{B4})$$

for  $N$  the number of possible outgoing movements from state  $j$ , which we assume to be independent of the current state, as is the case for our particular problem. In the case of the Metropolis-Hastings algorithm the detailed balance condition is fulfilled with the above definitions.

Having defined the Metropolis algorithm, we now want to quantize it using the previous section. There have been several proposals to quantize the Metropolis algorithm, as can be seen in the Appendix B. They often rely on slow evolution from  $|\pi_t\rangle \rightarrow |\pi_{t+1}\rangle$  using variations of Amplitude Amplification, until a large  $\beta$  has been achieved.

However, most often this Metropolis algorithms are used outside of equilibrium, something that is not often worked out in the previous approaches. There are at least two ways to perform the quantization of the out-of-equilibrium Metropolis-Hastings algorithm [21]. The first one, called ‘Zeno with rewind’ [19] uses a simpler version of previous quantum walks, where instead of amplitude amplification, quantum phase estimation is used on operators  $W_j$ , so that measuring the first eigenvalue means that we have prepared the corresponding eigenvector  $|\psi_t^0\rangle = |\pi_t\rangle$  [17]. Since the eigenvalue gap is  $\Delta_t$ , the cost of Quantum Phase Estimation is  $O(\Delta_t^{-1})$ .

Define measurements  $Q_t = |\pi_t\rangle \langle \pi_t|$  and  $Q_t^\perp = \mathbf{1} - |\pi_t\rangle \langle \pi_t|$ , for  $t$  an index indicating the step of the cooling schedule. Performing these measurements consists, as we have mentioned, in performing phase estimation of the corresponding operator  $\mathcal{W}_t$ , at cost  $\Delta_t^{-1}$ . If a measurement of type  $Q_t^\perp$  indicates a restart of the whole algorithm it is called ‘without rewind’. However, if measurement  $Q_t^\perp$  is obtained, one can perform phase estimation of  $\mathcal{W}_{t-1}$ . If  $|\langle \pi_t | \pi_{t-1} \rangle|^2 = F_t^2$ , then the transition probability between  $Q_j \leftrightarrow Q_{t-1}$  and between  $Q_t^\perp \leftrightarrow Q_{t-1}^\perp$  is given by  $F_t^2$ ; and the transition probability between  $Q_t \leftrightarrow Q_{t-1}^\perp$  and between  $Q_t^\perp \leftrightarrow Q_{t-1}$  is given by  $1 - F_t^2$ , so in a logarithmic number of steps one can recover state  $|\pi_{t-1}\rangle$  or  $|\pi_t\rangle$ .

The second proposal is to perform the unitary heuristic procedure [21]

$$|\psi(L)\rangle = W_L \dots W_1 |\pi_0\rangle. \quad (\text{B5})$$

This is in some ways the simplest way one would think of quantizing the Metropolis-Hastings algorithm, implementing a quantum walk instead of a random walk. It is very similar to the classical way of performing many steps of the classical walk, slowly increasing  $\beta$  until one arrives to the aim temperature. In addition, this procedure is significantly simpler than the previously explained ones because it does not require to perform phase estimation on  $W_t$ .

Two more innovations are introduced by [21]. In the first place, a heuristic Total Time to Solution (TTS) is defined. Assuming some start distribution if operators  $W$  are applied  $t$  times, the probability of success is given by  $p(t)$ . In order to be successful with constant probability  $1 - \delta$  that means repeating the procedure  $\log(1 - \delta) / \log(1 - p(t))$  times. The total expected time to success is then

$$TTS(t) := t \frac{\log(1 - \delta)}{\log(1 - p(t))}, \quad (\text{B6})$$

as also indicated in the main text equation (7). For the unitary procedure

$$TTS(L) = L \frac{\log(1 - \delta)}{\log(1 - |\langle \pi^g | W_L \dots W_1 | \pi_0 \rangle|^2)} \quad (\text{B7})$$

with  $\pi^g$  the ground state of the Hamiltonian.

Additionally [21] constructed an alternative to Szegedy operator  $\tilde{W}$  using a Boltzmann coin, such that the quantum walk operator operates on three registers  $|x\rangle_S |z\rangle_M |b\rangle_C$ .  $S$  stands for the codification of the state,  $M$  for the codification of possible movements, and  $C$  the Boltzmann coin. Their operator  $\tilde{W}$  is equivalent to the Szegedy operator under a conjugation operator  $Y$  that maps moves to states and viceversa:

$$\tilde{W} = RV^\dagger B^\dagger FBV, \quad (\text{B8})$$

with,

$$V : |0\rangle_M \rightarrow \sum_j N^{-1/2} |j\rangle \quad (\text{B9a})$$

$$B : |x\rangle_S |j\rangle_M |0\rangle_C \rightarrow |x\rangle_S |j\rangle_M \left( \sqrt{1 - A_{x \cdot z_j, x}} |0\rangle + \sqrt{A_{x \cdot z_j, x}} |1\rangle \right) \quad (\text{B9b})$$

$$F : |x\rangle_S |j\rangle_M |b\rangle_C \rightarrow |x \cdot z_j^b\rangle_S |j\rangle_M |b\rangle_C \quad (\text{B9c})$$

$$R : |0\rangle_M |0\rangle_C \rightarrow -|0\rangle_M |0\rangle_C \quad (B9d)$$

$$|j\rangle_M |b\rangle_C \rightarrow |j\rangle_M |b\rangle_C, \quad (j, b) \neq (0, 0)$$

Here  $V$  proposes different moves,  $B$  prepares the Boltzmann coin,  $F$  flips the bits necessary to prepare the new state, conditional on the Boltzmann

coin being in state 1, and  $R$  is a reflection operator on state  $(0, 0)$  for the coin and movement registers. Although our encoding of the operators and states is slightly different, the algorithm that we have used is this one, mainly due to its simplicity.

---

[1] U. Consortium, “Uniprot: a worldwide hub of protein knowledge,” *Nucleic Acids Research*, vol. 47, no. D1, pp. D506–D515, 2019.

[2] H. M. Berman, J. Westbrook, Z. Feng, G. Gilliland, T. N. Bhat, H. Weissig, I. N. Shindyalov, and P. E. Bourne, “The protein data bank,” *Nucleic Acids Research*, vol. 28, no. 1, pp. 235–242, 2000.

[3] N. Perdigão, J. Heinrich, C. Stolte, K. S. Sabir, M. J. Buckley, B. Tabor, B. Signal, B. S. Gloss, C. J. Hammang, B. Rost, *et al.*, “Unexpected features of the dark proteome,” *Proceedings of the National Academy of Sciences*, vol. 112, no. 52, pp. 15898–15903, 2015.

[4] A. Bhowmick, D. H. Brookes, S. R. Yost, H. J. Dyson, J. D. Forman-Kay, D. Gunter, M. Head-Gordon, G. L. Hura, V. S. Pande, D. E. Wemmer, *et al.*, “Finding our way in the dark proteome,” *Journal of the American Chemical Society*, vol. 138, no. 31, pp. 9730–9742, 2016.

[5] N. Perdigão and A. Rosa, “Dark proteome database: studies on dark proteins,” *High-throughput*, vol. 8, no. 2, p. 8, 2019.

[6] P. N. Bryan and J. Orban, “Proteins that switch folds,” *Current Opinion in Structural Biology*, vol. 20, no. 4, pp. 482–488, 2010.

[7] A. K. Dunker, J. D. Lawson, C. J. Brown, R. M. Williams, P. Romero, J. S. Oh, C. J. Oldfield, A. M. Campen, C. M. Ratliff, K. W. Hipps, *et al.*, “Intrinsically disordered protein,” *Journal of Molecular Graphics and Modelling*, vol. 19, no. 1, pp. 26–59, 2001.

[8] R. Das and D. Baker, “Macromolecular modeling with rosetta,” *Annu. Rev. Biochem.*, vol. 77, pp. 363–382, 2008.

[9] University of Washington, “Rosetta@home.” [boinc.bakerlab.org](http://boinc.bakerlab.org), 2021.

[10] R. Das, B. Qian, S. Raman, R. Vernon, J. Thompson, P. Bradley, S. Khare, M. D. Tyka, D. Bhat, D. Chivian, *et al.*, “Structure prediction for casp7 targets using extensive all-atom refinement with rosetta@ home,” *Proteins: Structure, Function, and Bioinformatics*, vol. 69, no. S8, pp. 118–128, 2007.

[11] W. E. Hart and S. Istrail, “Robust proofs of np-hardness for protein folding: general lattices and energy potentials,” *Journal of Computational Biology*, vol. 4, no. 1, pp. 1–22, 1997.

[12] B. Berger and T. Leighton, “Protein folding in the hydrophobic-hydrophilic (hp) is np-complete,” in *Proceedings of the Second Annual International Conference on Computational Molecular Biology*, pp. 30–39, 1998.

[13] A. Kryshtafovych, T. Schwede, M. Topf, K. Fidelis, and J. Moult, “Critical assessment of methods of protein structure prediction (casp)—round xiii,” *Proteins: Structure, Function, and Bioinformatics*, vol. 87, no. 12, pp. 1011–1020, 2019.

[14] A. Senior, R. Evans, J. Jumper, J. Kirkpatrick, L. Sifre, T. Green, C. Qin, A. Zidek, A. Nelson, A. Bridgland, *et al.*, “Improved protein structure prediction using potentials from deep learning,” *Nature*, 2020.

[15] M. D. Hanwell, D. E. Curtis, D. C. Lonie, T. Vandevoorde, E. Zurek, and G. R. Hutchison, “Avogadro: an advanced semantic chemical editor, visualization, and analysis platform,” *Journal of Chemical Informatics*, vol. 4, no. 1, p. 17, 2012.

[16] P. Wocjan and A. Abeyesinghe, “Speedup via quantum sampling,” *Physical Review A*, vol. 78, no. 4, p. 042336, 2008.

[17] R. Somma, S. Boixo, and H. Barnum, “Quantum simulated annealing,” *arXiv preprint arXiv:0712.1008*, 2007.

[18] R. D. Somma, S. Boixo, H. Barnum, and E. Knill, “Quantum simulations of classical annealing processes,” *Physical Review Letters*, vol. 101, no. 13, p. 130504, 2008.

[19] K. Temme, T. J. Osborne, K. G. Vollbrecht, D. Poulin, and F. Verstraete, “Quantum metropolis sampling,” *Nature*, vol. 471, no. 7336, p. 87, 2011.

[20] M.-H. Yung and A. Aspuru-Guzik, “A quantum-quantum metropolis algorithm,” *Proceedings of the National Academy of Sciences*, vol. 109, no. 3, pp. 754–759, 2012.

[21] J. Lemieux, B. Heim, D. Poulin, K. Svore, and M. Troyer, “Efficient Quantum Walk Circuits for Metropolis-Hastings Algorithm,” *Quantum*, vol. 4, p. 287, June 2020.

[22] M. Szegedy, “Quantum speed-up of markov chain based algorithms,” in *45th Annual IEEE Symposium on Foundations of Computer Science*, pp. 32–41, IEEE, 2004.

[23] R. Babbush, A. Perdomo-Ortiz, B. O’Gorman, W. Macready, and A. Aspuru-Guzik, “Construction of energy functions for lattice heteropolymer models: a case study in constraint satisfaction programming and adiabatic quantum optimization,” *arXiv preprint arXiv:1211.3422*, 2012.

[24] A. Robert, P. K. Barkoutsos, S. Woerner, and I. Tavernelli, “Resource-efficient quantum algorithm for protein folding,” *arXiv preprint arXiv:1908.02163*, 2019.

[25] A. Perdomo-Ortiz, N. Dickson, M. Drew-Brook,

G. Rose, and A. Aspuru-Guzik, “Finding low-energy conformations of lattice protein models by quantum annealing,” *Scientific Reports*, vol. 2, p. 571, 2012.

[26] M. Fingerhuth, T. Babej, *et al.*, “A quantum alternating operator ansatz with hard and soft constraints for lattice protein folding,” *arXiv preprint arXiv:1810.13411*, 2018.

[27] T. Babej, M. Fingerhuth, *et al.*, “Coarse-grained lattice protein folding on a quantum annealer,” *arXiv preprint arXiv:1811.00713*, 2018.

[28] A. Perdomo, C. Truncik, I. Tubert-Brohman, G. Rose, and A. Aspuru-Guzik, “Construction of model hamiltonians for adiabatic quantum computation and its application to finding low-energy conformations of lattice protein models,” *Physical Review A*, vol. 78, no. 1, p. 012320, 2008.

[29] C. Outeiral, G. M. Morris, J. Shi, M. Strahm, S. C. Benjamin, and C. M. Deane, “Investigating the potential for a limited quantum speedup on protein lattice problems,” *arXiv preprint arXiv:2004.01118*, 2020.

[30] V. K. Mulligan, H. Melo, H. I. Merritt, S. Slocum, B. D. Weitzner, A. M. Watkins, P. D. Renfrew, C. Pelissier, P. S. Arora, and R. Bonneau, “Designing peptides on a quantum computer,” *bioRxiv*, p. 752485, 2020.

[31] L. Banchi, M. Fingerhuth, T. Babej, C. Ing, and J. M. Arrazola, “Molecular docking with gaussian boson sampling,” *Science Advances*, vol. 6, no. 23, p. eaax1950, 2020.

[32] The  $\alpha$ -helix and the  $\beta$ -sheet correspond to two common structures found in protein folding. Such structures constitute what is called the secondary structure of the protein, and are characterised because  $(\phi, \psi) = (-\pi/3, -\pi/4)$  in the  $\alpha$ -helix, and  $(\phi, \psi) = (-3\pi/4, -3\pi/4)$  in the  $\beta$ -sheet, due to the hydrogen bonds that happen between backbone amino groups NH and backbone carboxy groups CO.

[33] R. Von Mises, *Mathematical Theory of Probability and Statistics*. Academic Press, 2014.

[34] J. M. Turney, A. C. Simmonett, R. M. Parrish, E. G. Hohenstein, F. A. Evangelista, J. T. Fermann, B. J. Mintz, L. A. Burns, J. J. Wilke, M. L. Abrams, *et al.*, “Psi4: an open-source ab initio electronic structure program,” *Wiley Interdisciplinary Reviews: Computational Molecular Science*, vol. 2, no. 4, pp. 556–565, 2012.

[35] L. K. Grover, “Quantum mechanics helps in searching for a needle in a haystack,” *Physical Review Letters*, vol. 79, no. 2, p. 325, 1997.

[36] F. Magniez, A. Nayak, J. Roland, and M. Santha, “Search via quantum walk,” *SIAM Journal on Computing*, vol. 40, no. 1, pp. 142–164, 2011.

[37] T. Albash and D. A. Lidar, “Demonstration of a scaling advantage for a quantum annealer over simulated annealing,” *Physical Review X*, vol. 8, no. 3, p. 031016, 2018.

[38] E. Alcaide, “Minifold: a deeplearning-based mini protein folding engine.” <https://github.com/EricAlcaide/MiniFold/>, 2019.

[39] H. Abraham *et al.*, “Qiskit: An open-source framework for quantum computing,” 2019.

[40] Amazon.com, Inc., “Amazon web services.” [aws.amazon.com](https://aws.amazon.com), 2021.

[41] S. Kim, J. Chen, T. Cheng, A. Gindulyte, J. He, S. He, Q. Li, B. A. Shoemaker, P. A. Thiessen, B. Yu, *et al.*, “Pubchem 2019 update: improved access to chemical data,” *Nucleic Acids Research*, vol. 47, no. D1, pp. D1102–D1109, 2019.

[42] F. Jensen, “Atomic orbital basis sets,” *Wiley Interdisciplinary Reviews: Computational Molecular Science*, vol. 3, no. 3, pp. 273–295, 2013.

[43] T. Helgaker, P. Jorgensen, and J. Olsen, *Molecular electronic-structure theory*. John Wiley & Sons, 2014.

[44] L. Grover and T. Rudolph, “Creating superpositions that correspond to efficiently integrable probability distributions,” *arXiv preprint quant-ph/0208112*, 2002.

[45] S. Kirkpatrick, C. D. Gelatt, and M. P. Vecchi, “Optimization by simulated annealing,” *Science*, vol. 220, no. 4598, pp. 671–680, 1983.

[46] K. Temme, S. Bravyi, and J. M. Gambetta, “Error mitigation for short-depth quantum circuits,” *Physical Review Letters*, vol. 119, no. 18, p. 180509, 2017.

[47] R. LaRose, A. Mari, P. J. Karalekas, N. Shammah, and W. J. Zeng, “Mitiq: A software package for error mitigation on noisy quantum computers,” 2020.

[48] M. Abadi, P. Barham, J. Chen, Z. Chen, A. Davis, J. Dean, M. Devin, S. Ghemawat, G. Irving, M. Isard, *et al.*, “Tensorflow: A system for large-scale machine learning,” in *12th {USENIX} Symposium on Operating Systems Design and Implementation ({OSDI} 16)*, pp. 265–283, 2016.

[49] F. Chollet *et al.*, “Keras.” <https://github.com/fchollet/keras>, 2015.

[50] R. S. Sutton and A. G. Barto, *Reinforcement learning: An introduction*. MIT press, 2018.

[51] P. J. Van Laarhoven and E. H. Aarts, “Simulated annealing,” in *Simulated annealing: Theory and applications*, pp. 7–15, Springer, 1987.

[52] Student, “The probable error of a mean,” *Biometrika*, pp. 1–25, 1908.

[53] R. Portugal, *Quantum walks and search algorithms*. Springer, 2013.

[54] A. Ambainis, “Quantum walk algorithm for element distinctness,” *SIAM Journal on Computing*, vol. 37, no. 1, pp. 210–239, 2007.

[55] G. D. Paparo and M. Martin-Delgado, “Google in a quantum network,” *Scientific Reports*, vol. 2, p. 444, 2012.

[56] G. D. Paparo, M. Müller, F. Comellas, and M. A. Martin-Delgado, “Quantum google in a complex network,” *Scientific Reports*, vol. 3, p. 2773, 2013.

[57] G. D. Paparo, V. Dunjko, A. Makmal, M. A. Martin-Delgado, and H. J. Briegel, “Quantum speedup for active learning agents,” *Physical Review X*, vol. 4, no. 3, p. 031002, 2014.

[58] Notice that in most texts the definition of  $M$  does not explicitly include  $S$ . It is assumed implicitly though.